

Multi-class Road Defect Detection and Segmentation using Spatial and Channel-wise Attention for Autonomous Road Repairing

Jongmin Yu^{1,2}, Chen Bene Chi³, Sebastiano Fichera^{4,5},
Paolo Paoletti^{4,5}, Devansh Mehta⁴, and Shan Luo^{2,†}

Abstract—Road pavement detection and segmentation are critical for developing autonomous road repair systems. However, developing an instance segmentation method that simultaneously performs multi-class defect detection and segmentation is challenging due to the textural simplicity of road pavement image, the diversity of defect geometries, and the morphological ambiguity between classes. We propose a novel end-to-end method for multi-class road defect detection and segmentation. The proposed method comprises multiple spatial and channel-wise attention blocks available to learn global representations across spatial and channel-wise dimensions. Through these attention blocks, more globally generalised representations of morphological information (spatial characteristics) of road defects and colour and depth information of images can be learned. To demonstrate the effectiveness of our framework, we conducted various ablation studies and comparisons with prior methods on a newly collected dataset annotated with nine road defect classes. The experiments show that our proposed method outperforms existing state-of-the-art methods for multi-class road defect detection and segmentation methods.

I. INTRODUCTION

Bad road conditions pose multiple problems: they contribute to vehicle damage, cause nearly 13% of car accidents in the UK [1], increase carbon emissions [2], and lead to higher fuel consumption [3]. Currently, human workers usually handle road repairs, which is both dangerous and inefficient. Emerging technologies are looking to employ machines powered by advanced computer vision algorithms. These algorithms use object detection and segmentation techniques to accurately identify and mark road defects. Proper road defect detection ensures that the repair machines can locate precisely where the issues are, while segmentation helps in understanding the extent of the defect, thereby optimising the amount of repair material needed [4], [5]. Therefore, developing precise object detection and segmentation methods

¹Department of Applied Mathematics and Theoretical Physics, University of Cambridge, Wilberforce Rd, Cambridge CB3 0WA, United Kingdom jy522@cam.ac.uk (was affiliated with Department of Engineering, King’s College London, Strand, London, WC2R 2LS, United Kingdom).

²Department of Engineering, King’s College London, Strand, London, WC2R 2LS, United Kingdom, shan.luo@kcl.ac.uk.

³Department of Informatics, King’s College London, Strand, London, WC2R 2LS, United Kingdom, chi.b.chen@kcl.ac.uk.

⁴Robotiz3D, Sci-Tech Daresbury Keckwick Lane, WA4 4FS, United Kingdom, {devansh.mehta}@robotiz3d.com

⁵School of Engineering, University of Liverpool, Brownlow Hill, L69 3GH, Liverpool, United Kingdom, {sebastiano.fichera, paoletti}@liverpool.ac.uk

This work was supported by the Innovate UK SMART grant “ARRES PREVENT: The World-First Autonomous Road Repair Vehicle” (10006122).

† represents the corresponding author.

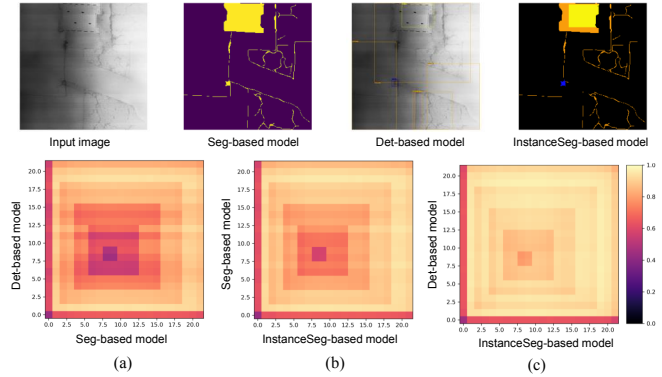


Fig. 1: Visualisation of Kernel similarities computed based on Centered Kernel Alignment (CKA) [6]. (a) denotes the kernel similarity map for segmentation (Seg-based model) and detection (Det-based model) models. (b) denotes the kernel similarity map for segmentation and instance segmentation (InstanceSeg-based model) models. (c) denotes the kernel similarity map for detection and instance segmentation models. Each axis denotes the depth of layers. The brighter the colour, the higher the kernel similarity.

is crucial for making these automated road repair systems effective and cost-efficient.

Numerous methods have been proposed for road defect segmentation, showing considerable success for publicly available datasets [7]–[10]. It can be thought that methodological advancements alongside deep learning technologies led to these achievements. However, it can not be denied that the distinct colours and textures of road defects are compared to normal surfaces. Multi-class road defect detection still faces challenges because of diverse defect geometries and morphological ambiguities between classes. While recent deep learning methods have shown promise [11]–[13], they struggle with limitations such as detecting defects at the image unit level (*i.e.*, distinguishing whether defects exist in an image) [12] or focusing on defect classes that are easy to be identified [11], [13]. To perform the segmentation and detection simultaneously, some studies utilise instance segmentation approaches [14]–[16]. However, unlike general approaches of instance segmentation [17]–[19], it takes the form of a two-stage framework that crops images after detection and then proceeds with segmentation for each image.

In addressing road defect segmentation and detection within a single framework, the network must adeptly learn colour attributes useful for segmentation and spatial information crucial for multi-class detection. Based on the Mask-RCNN [17] structure, we analyse the kernel similarities measured by Centered Kernel Alignment (CKA) [6] between three models

trained by segmentation, detection, and instance segmentation objectives. We find out that the model trained by an instant segmentation objective is more similar to the model trained by a detection objective (See Fig. 1, the colour of kernel similarity map between the detection model and the instance segmentation model (Fig. 1(c)) is lighter than the kernel similarity map between the instant model and segmentation model (Fig. 1(b))). This indicates that the learned kernels may be biased in the detection information. As a result, these disparities have necessitated a two-stage framework design in prior studies [14]–[16]. However, this two-stage approach undermines computational efficiency since the computational time for the segmentation depends on detection results.

To overcome this, we introduce a novel Spatial and Channel-wise Multi-head Attention Mask-RCNN (SCM-MRCNN) for detecting and segmenting multi-road defect classes. Built upon the foundation of MRCNN, SCM-MRCNN incorporates Spatial and Channel-wise Multi-head Attention (SCM-attention) blocks. These blocks are designed to extract latent features broadly robust to variations in geometric shape and colour information of road defects within a given image. Not only is the attention mechanism applied across the spatial domain, but similar techniques are applied to the channel axis to extract features with enhanced generalisation of both the spatial and channel axes. Ablation studies show that SCM attention improves multi-class defect detection and segmentation performance.

Additionally, we introduce a new dataset named the RoadEYE to provide a new benchmark for multi-class road defect detection and segmentation. Unlike existing road defect detection datasets [11] that only provide detection labels in the form of bounding boxes for multiple classes, or other general segmentation datasets [20] that consider all defects as a single class without class distinction, the proposed dataset provides bounding for multi-class road defects. We provide a new benchmark for multi-class defect detection and segmentation research by providing box-shaped and segmentation labels for six classes of road defects. We conduct extensive experiments to demonstrate the proposed SCM-Attention block’s efficacy and evaluate its performance in multi-class road defect detection and segmentation. The SCM-MRCNN achieves a mean average precision (mAP) of 61.7% on the RDD2020 dataset [11]. For defect segmentation, the SCM-MRCNN achieves an average intersection over union (AIU) of 53.1% on the Surface Crack dataset [20]. Experimental results on the RoadEYE dataset indicate that SCM-MRCNN outperforms the state-of-the-art (SOTA) method [21] by 1.8% in multi-class road defect detection and segmentation.

Our key contributions are as follows:

- A spatial and channel-wise multi-head attention Mask-RCNN (SCM-MRCNN), the first unified framework for multi-class road defect detection and segmentation.
- The proposed Spatial and Channel-wise attention block can learn more global representation for both spatial and channel-wise dimensions.
- A new multi-class road defect detection and segmentation dataset (RoadEYE dataset) is collected and annotated.

Before 2008, defect detection relied on signal filtering [22], [23] using pixel values, assuming “cracks are deeper than surroundings”. The algorithm differentiated cracks and roads via these methods, achieving 95.5% success in feature-based filtering [23]–[25]. This involved pre-defined defect descriptions and layered thresholding. Yet, these methods have limitations. They’re adept mainly at detecting one specific type of crack, often struggling with noise and differentiating cracks from similar-shaped objects, especially in low-contrast settings. Adapting them for new tasks or defects is challenging due to their reliance on thresholding-defined crack features [26], necessitating significant rework.

Machine learning techniques, when combined with hand-crafted features, address road image classification challenges. These techniques utilise various extractors to discern road defects. [27] They are more adaptable than traditional methods, with the suitable feature extractor producing solid results. [28] Using varied feature extractors and Adaboost enhances defect detection on multiple surfaces. While traditional algorithms like Random Forest are utilised [29], SVM has become prominent recently due to its noise-reduction capabilities. [30] However, these methods face challenges. The effectiveness of hand-crafted features can significantly influence performance. Moreover, traditional machine learning cannot often extract high-level features efficiently.

Deep learning revolutionised feature extraction compared to traditional machine learning, automatically extracting features in a stable and generalised manner, reducing adaptation effort for new tasks. Early models like Artificial Neural Networks (ANNs) detected image cracks but were computationally demanding [31], [32]. Convolution Neural Networks (CNNs) enable efficient whole-image processing in computer vision. Multi-layer CNNs like FCN, with multi-scale feature extraction [33] or multiple labelled source domains [34], improved performance. However, CNNs have limitations: they simultaneously struggle with pixel nuances and global context and face class imbalance issues, making them less suitable for multi-class tasks. Therefore, researchers proposed deep-learning based solutions.

To address road defect segmentation, methods combine CNN and attention mechanism proposed [35]–[37]. Attention mechanisms enable the network to emphasise crucial parts and reduce the weight of background pixels. Transformers, using self-attention mechanisms [38], are employed for segmentation. Several methods integrate CNN with the transformer, achieving high performance [39]–[41]. However, concerns have been raised about their inference speed [42], necessitating extra effort to utilise these solutions for instant road defect segmentation.

In the domain of road defect detection and classification, the introduction of RCNN (Region-Based Convolutional Neural Network) [43] represented a notable breakthrough, albeit with the drawback of relying on an extensive 2,000 region proposal process that impeded real-time performance. Subsequent iterations like Fast-RCNN [44] and Faster-RCNN [45]–[48]

addressed this limitation by integrating automatic region-proposing methods, significantly reducing training time, and advancing towards real-time road defect detection. Mask-RCNN [17] further extends Faster-RCNN by introducing object segmentation capabilities, enhancing its suitability for instant road defect detection and segmentation.

III. THE PROPOSED METHOD

A. Method Overview

As mentioned in Section I and shown in Fig. 1, General MRCNN tend to be biased into detection objectives regarding learning a multi-class road defect detection and segmentation method. The model should learn spatially and channel-wise robust representation to produce a good segmentation and detection performance using a single framework. As illustrated in Fig. 2a, the architecture of our proposed SCM-MRCNN is inspired by MRCNN [17]. SCM-attention block is placed between the convolutional and deconvolutional layers. The convolutional and deconvolutional layers are used to down-sample or up-sample the features. SCM-attention blocks have been located in between each convolutional or deconvolutional layer to reinforce spatial and channel-wise robustness of learnt features.

To learn spatially and channel-wisely more robust representation for multi-class road defect detection and segmentation, we propose a new spatial and channel-wise multi-head attention (SCM attention) block to fuse the advantage of the long dependency modelling in Transformer and channel-wise attention. The SCM attention block comprises two steps: patch-level channel attention and multi-head attention.

Patch-level Channel Attention: Given the features extracted from each convolutional or deconvolutional layers $\mathbf{O} \in \mathbb{R}^{H \times W \times C_i}$, ($i = 1, 2, 3, \dots, n$), we first make a set of small-size patch by splitting the features using pre-defined patch sizes P . This process is only conducted for spatial dimension so that we keep the original channel dimensions through this process $\mathbf{O} = \{o_i\}_{i=1:n_p}$, where n_p is the number of patches. Then, we reshape each patch into a 2D flattened shape $\bar{o}_i \in \mathcal{R}^{hw \times C}$. We compute the channel-attention matrix \mathbf{m} by multiplying the reshaped patch and fusing the matrix with the original patch $\mathbf{m} = \bar{o}_i \bar{o}_i^T$. Channel-wise attention feature is finally obtained by applying the softmax function across the channel axes of the fused patch, and residual structure is applied to encode channel and dependencies for refining features from each latent feature, as follows:

$$\begin{aligned} \hat{o}_i &= o_i + \sigma(\mathbf{m}o_i) \\ &= o_i + \sigma(\bar{o}_i \bar{o}_i^T o_i) \end{aligned} \quad (1)$$

Fig. 2c represents the detailed process of the patch-level channel attention. After finishing the patch-level channel attention, outputs are applied to the multi-head attention to learn spatially reinforced features.

Multi-head Attention: We conduct the tokenisation of the outputs of the patch-level channel attention by reshaping the features into sequences of flattened 2D patches. Positional encoding is applied to each token. The tokens are then fed into the multi-head cross-attention layer (See Fig. 2b), followed

by a Multi-Layer Perceptron (MLP) with residual structure to encode channel and dependencies for refining features from each latent feature.

Each token \mathbf{T}_i is applied to multi-head attention by defining queries \mathbf{Q}_i , key \mathbf{K}_i , and value \mathbf{V}_i :

$$\mathbf{Q}_i = \mathbf{T}_i W_{\mathbf{Q}_i}, \mathbf{K}_i = \mathbf{T}_i W_{\mathbf{K}}, \mathbf{V}_i = \mathbf{T}_i W_{\mathbf{V}} \quad (2)$$

where $W_{\mathbf{Q}_i} \in \mathbb{R}^{C_i \times d}$, $W_{\mathbf{K}} \in \mathbb{R}^{C_i \times d}$, $W_{\mathbf{V}} \in \mathbb{R}^{C_i \times d}$ are kernels for mapping the key, value, and queries. d denotes the sequence length (patch numbers).

With $\mathbf{Q}_i \in \mathbb{R}^{C_i \times d}$, $\mathbf{K} \in \mathbb{R}^{C_\Sigma \times d}$, $\mathbf{V} \in \mathbb{R}^{C_\Sigma \times d}$, the attention matrix \mathbf{M}_i are produced and the value \mathbf{V} is weighted by \mathbf{M}_i through a self-attention mechanism:

$$\mathbf{A}_i = \mathbf{M}_i \mathbf{V}^\top = \sigma \left[\psi \left(\frac{\mathbf{Q}_i^\top \mathbf{K}_\Sigma}{\sqrt{C_i}} \right) \right] \mathbf{V}_i^\top \quad (3)$$

where \mathbf{K}_Σ defines a matrix storing the keys: $\mathbf{K}_\Sigma = \{\mathbf{K}_i\}_{i=1:d}$ and $\mathbf{K}_\Sigma \in \mathcal{R}^{d \times d}$. $\psi(\cdot)$ and $\sigma(\cdot)$ denote the instance normalisation [49] and the softmax function, respectively.

In a multi-head attention with N -heads, the output is calculated as follows:

$$\mathbf{MA}_i = (\mathbf{A}_i^1 + \mathbf{A}_i^2 + \dots + \mathbf{A}_i^N) / N \quad (4)$$

Hereinafter, applying an MLP and residual operator, the output is obtained as follows:

$$\mathbf{O}_i = \mathbf{MA}_i + \text{MLP}(\mathbf{MA}_i) \quad (5)$$

For simplicity, we omitted the layer normalisation (See Layer Norm blocks in Fig 2b) in equation descriptions. The operation of the SCM attention blocks can be repeated multiple times to build a multi-layer attention block. In our implementation, the number of heads for multi-head attention and the number of SCM attention layers are set to 4 and 2, respectively. We empirically found that the four layers and two heads can achieve the best performance in our experiment.

B. Training and Instance Segmentation

To train the end-to-end method for multi-class road defect detection and segmentation, we minimise a multi-task objective function consisting of the multi-class detection loss and L_{Det} and binary segmentation loss \mathcal{L}^{Seg} .

First, the multi-class detection loss L_{Det} is defined as:

$$\begin{aligned} L_{\text{Det}}(\{p_i\}, \{t_i\}) &= \frac{1}{N_{\text{anch}}} \sum_i (L_{\text{p-cls}}(p_i^*, p_i^p) + L_{\text{m-cls}}(p_i, p_i^c)) \\ &\quad + \lambda \frac{1}{N_{\text{anch}}} \sum_i p_i^* L_{\text{reg}}(t_i, t_i^*). \end{aligned} \quad (6)$$

Here, i is the index of an anchor in each mini-batch, and p_i is the predicted probability of anchor i being a particular class's object. $L_{\text{p-cls}}$ is log loss related to object existence, so it is computed over two classes (object vs not object). The ground-truth labels related to object existence p_i^p is one if the anchor is positive and 0 if the anchor is negative. $L_{\text{m-cls}}$ is applied for classifying defect classes so that the ground-truth labels for object classes p_i^c are defined by a one-hot

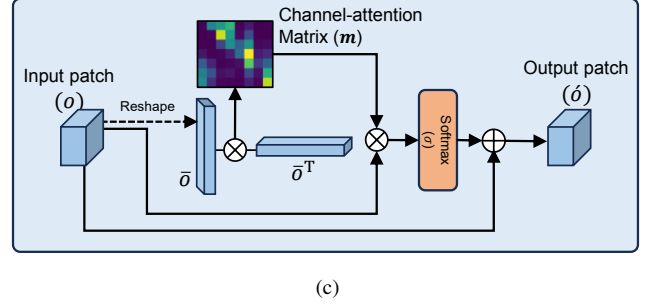
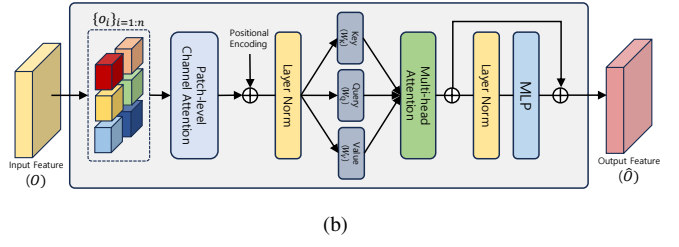
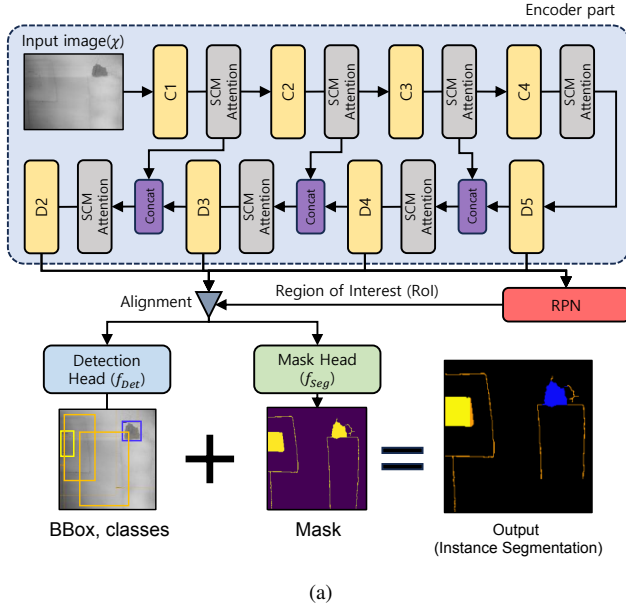


Fig. 2: Structural details of the proposed SCM-MRCNN and SCM attention block. (a) denotes Architectural details of the proposed SCM. C# and D# denote convolutional and deconvolutional layers, respectively. 'Concat' represents a concatenating operation between two latent features. (b) and (c) represents the structural details of the proposed spatial and channel-wise multi-head attention (SCM-attention) block and patch-based channel attention, respectively. \otimes and \oplus denote element-wise multiplication and element-wise addition, respectively.

vector representing a particular object class. p_i^* is defined by the maximum value among the predicted probability of the classification output. t_i is a vector representing the four parameterised coordinates of the predicted bounding box, and t_i^* is that of the ground-truth box.

For the bounding box regression, we use $L_{\text{reg}}(t_i, t_i^*) = R(t_i - t_i^*)$ where R is the robust loss function (smooth L_1). The term $p_i^* L_{\text{reg}}$ means the regression loss is activated only for positive anchors ($p_i^* = 1$) and is disabled otherwise ($p_i^* = 0$). Those loss terms are regularised by N_{cls} and N_{reg} and weighted by a balancing parameter λ .

Second, the loss function for the segmentation head is defined by the combination of binary-cross entropy loss and dice loss, as follows:

$$\mathcal{L}_{\text{Seg}}(\{o_i\}, \{\hat{o}_i\}) = \sum_i (L_{\text{bce}}(o_i, \hat{o}_i) + L_{\text{dice}}(o_i, \hat{o}_i)), \quad (7)$$

where o_i and \hat{o}_i indicate the binary segmentation results and pixel-level annotation for each road defect. The reason why the defect division is divided into dual classes rather than multi-classes is as follows. As mentioned before, defects on the road surface have similar colours regardless of class, and if you try to distinguish them forcibly, the performance may deteriorate. In some cases, road defects are connected, and clearly distinguishing them is very difficult, even for experts with pixel-level labels.

In optimising the entire framework, except for the standard part that extracts the features corresponding to each head as input (the encoding part, See Fig. 2a), the remaining parts (the network corresponding to each head) do not share the gradient of each loss function. Only the encoding part is jointly trained, and the detection and segmentation head are optimised independently.

The instance segmentation process for multi-class road defects using SCM-MRCNN is performed by combining the detection and segmentation results of the segment head. The segmentation areas for multi-class road defects are divided based on the detection bounding box first. Then, the class assignment for each segment area has the highest probability among the detection results of the detection head (p_i^* in Eq. 6), which is assigned to the output class. If several detection results exist, classes are allocated sequentially from the detection result with the highest class probability.

IV. EXPERIMENTAL RESULTS

A. Dataset and evaluation metrics

There is no benchmark for evaluating the multi-class road defect detection and segmentation performances; Therefore, we utilise defect segmentation datasets [50] and road defect detection dataset [11], which are publicly available. Also, we created the RoadEYE dataset as a novel benchmark for multi-class road defect detection and segmentation. The descriptions of those datasets are as follows:

Crack Segmentation Dataset is merged from 11 crack segmentation datasets [51]. The dataset contains 11,200 images. All the images are resized to the size of 448×448 , and include RGB channels. The two folders of images and masks contain all the images. The two folders, train and test, contain training and testing images split from the two above folders. The splitting is stratified so that the proportion of each dataset in the train and test folder is similar.

RDD2020 dataset is created by [11], and it is a large-scale dataset that comprises 26,336 road images captured in India, Japan, and the Czech Republic. The dataset includes over 31,000 instances of road damage and is designed for developing deep learning-based methods to detect and classify

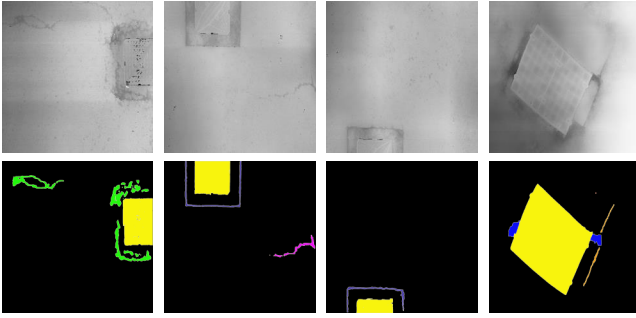


Fig. 3: Example snapshots of a sample of the RoadEYE dataset. Top: images. Bottom: Annotation of instance segmentation for multi-class road defect detection and segmentation.

	Pothole	Manhole	Longitudinal	Transverse	Joint	Wheel	Total
#	253	172	182	101	184	248	1140
%	22.2	15.1	16.0	8.9	16.1	21.8	100

TABLE I: The proportions (%) and number (#) of instances corresponding to each defect class.

various types of road damage automatically. RDD2020 covers a range of common road damage types, such as longitudinal cracks, transverse cracks, alligator cracks, and potholes. The dataset includes images with resolutions of either 600×600 or 720×720 , providing a detailed view of the road surface. **RoadEYE dataset**¹ is a new benchmark for multi-class road defect detection and segmentation. We captured 1,404 road surface point clouds to create the dataset and generated grey-scaled images. We selected 407 images that contain road defects for labelling. Each sample of a road surface image, segmentation mask, and annotation file for detection bounding boxes. We classified numerous road defects into nine defect classes. Fig. 3 and Table I show the example snapshot of a sample and statistics of the RoadEYE dataset. The dataset is the first to provide segmentation masks and bounding box annotations for the six road defect classes.

This work performs performance evaluation in three areas: Binary-class segmentation, multi-class defect detection, and instance segmentation (*i.e.*, multi-class defect detection and segmentation). All defect classes are considered one class for evaluating the binary-class segmentation. Average Intersection over Union (AIU), Optimal Dataset Scale (ODS), and Optimal Image Scale (OIS) are used for the evaluation metrics. The multi-class defect detection’s performance is evaluated using precision, recall, F1-score, and average precision (AP). The performance evaluation for the instant segmentation performance is conducted based on the average precision computed based on the segmentation mask (AP_M) and bounding boxes (AP_B).

B. Implementation

The segmentation loss \mathcal{L}_{Seg} is defined only for positive detection results. The mask target is the intersection between a ROI and its associated ground truth. The results will be considered positive when IoU between a detected bounding

¹To access the dataset, please visit <https://github.com/Robotiz3d/dataset>

Naive-MRCNN			SM-MRCNN			SCM-MRCNN		
AIU	AP_M	AP_B	AIU	AP_M	AP_B	AIU	AP_M	AP_B
When \mathcal{L}_{Seg} considers multi-class segmentation								
4.7	32.5	62.5	7.4	51.6	69.3	9.4	61.5	72.7
When \mathcal{L}_{Seg} considers binary-class segmentation								
15.5	60.6	68.0	18.6	64.1	70.4	22.6	68.6	73.3

TABLE II: Performance evaluation results depending on architecture configuration and loss function settings on the RoadEYE dataset.

box and corresponding annotation is over 0.5. The resolution of images is resized to 224×224 . A stochastic gradient descent (SGD) is used for optimising parameters. The batch size is set by 4. To obtain experimental results for the three datasets, we train each dataset for 200 epochs, with a starting learning rate of 0.01. Learning rate decay is applied so that it is decreased by multiplying it by 0.99 for every 20 epoch.

C. Ablation study

The SCM-MRCNN has two remarkable changes compared with the original MRCNN [17]. First, in training the SCM-MRCNN, we applied a binary segmentation strategy for the segmentation head (f_{Seg}). Instead of cross-entropy loss for multi-class segmentation, we applied combination loss of the binary cross entropy and dice loss (See Eq. 7). Second, as shown in Fig. 2a, the SCM attention blocks have been embedded between each convolutional or deconvolutional layer to learn a robust representation spatially and channel-wise. We have conducted ablation studies to demonstrate the effectiveness of those critical changes.

Table II presents the evaluation results depending on loss function settings and architectural configurations. Training a segmentation head using a binary-class segmentation setting is more beneficial for multi-class road defect detection and segmentation. The MRCNNs trained by the binary-class segmentation outperform counterparts with significant performance gaps *e.g.*, Naive-MRCNN trained by the multi-class segmentation settings produces 4.7 AIU and 32.5 AP_M ; however, it obtains 15.5 AIU and 60.6 AP_M when the binary-class segmentation setting trains it.

In terms of the performance analysis concerning the architectural configuration, we compare the average precision computed based on segmentation mask (AP_M) and detection bounding box (AP_B). MRCNN without structural modification (Naive-MRCNN) achieves AP_M of 60.6 and AP_B of 68.0. These are the lowest performance. MRCNN with spatial multi-head attention (SM-MRCNN) and the MRCNN with SCM attention block (SCM-MRCNN) achieve better performance.

D. Comparison with existing methods

The proposed SCM-MRCNN can provide three outputs: 1) Multi-class detection, 2) Binary segmentation, and 3) instance segmentation. We compare the performance of our method in terms of all the aforementioned aspects, respectively. The methods we have chosen for comparison include detection and segmentation methods for road defects and building defects [13], [52]–[54] in a similar domain. Additionally, because our method can be classified as an instant segmentation method,

Methods	Crack Segmentation [20]			RoadEYE		
	AIU	ODS	OIS	AIU	ODS	OIS
MRCNN (f_{Seg}) [52]	48.9	62.3	66.8	15.3	55.3	58.6
RCF [52]	46.7	53.2	60.3	19.6	51.7	60.2
FCN [53]	38.1	50.9	58.6	10.8	51.6	41.9
FPHBN [54]	50.1	61.7	65.0	10.3	53.3	55.4
U-Net [55]	46.7	49.3	55.2	19.3	41.2	38.2
DeepCrack [54]	45.6	59.1	53.2	17.6	49.2	27.6
Dual-Swin [18]	52.8	64.3	68.7	20.5	52.4	51.6
SCM-MRCNN (f_{Seg})	53.1	64.5	69.0	22.6	58.7	56.4

TABLE III: Quantitative comparison for the road defect segmentation performance using Crack Segmentation dataset and RoadEYE dataset. The **bolded** numbers indicate the best performance.

Methods	RDD2020 [11]				RoadEYE			
	Precision	Recall	F1	mAP	Precision	Recall	F1	mAP
MRCNN (f_{Det}) [52]	61.3	58.7	59.3	59.3	62.7	58.5	59.3	61.7
Faster-RCNN [53]	62.7	59.3	60.1	60.2	64.2	59.1	60.9	62.4
Yolov5 [54]	58.5	57.3	57.8	57.2	58.5	55.3	55.9	57.8
SSD [55]	57.9	57.1	57.3	56.3	60.9	56.0	56.4	57.5
Zhang <i>et al.</i> [12]	58.3	57.5	56.4	56.5	61.7	57.7	58.9	60.2
YOLO-LRDD [13]	59.2	58.2	58.7	57.6	60.3	56.9	57.5	58.3
SCM-MRCNN (f_{Det})	63.5	60.9	61.5	61.7	65.4	61.3	62.7	63.1

TABLE IV: Quantitative comparison for the multi-class road defect detection performance using RDD2020 dataset [56] and RoadEYE dataset. The **bolded** numbers indicate the best performance.

Method	Params	FPS	Pothole		Manhole		Longitudinal		Transverse		Joint		Wheel		mAP	
			AP _M	AP _B												
MRCNN [17]	44 M	11.7	77.8	86.3	74.2	82.1	65.2	76.4	54.2	60.5	38.2	42.3	54.0	60.3	60.6	68.0
Mask Transfiner [57]	44 M	13.1	81.2	84.6	79.4	81.6	58.1	62.3	52.3	58.2	40.2	43.6	55.2	58.2	61.1	64.8
Dual-Swin [18]	107 M	7.4	84.1	90.4	76.6	84.3	75.3	85.2	57.2	61.8	38.1	39.6	58.8	59.2	65.1	70.1
YOLACT [21]	114 M	21.7	67.3	69.3	71.1	73.2	61.5	66.7	42.7	46.3	21.7	22.8	36.2	40.1	50.1	53.1
Centermask [19]	114 M	8.4	73.0	79.5	75.2	80.2	76.1	80.9	51.4	56.9	20.6	23.5	47.1	48.2	57.2	61.5
He <i>et al.</i> [14]	65 M	8.5	72.4	74.2	73.0	76.3	62.1	65.4	44.8	48.1	27.5	30.6	51.7	55.7	55.2	58.3
Zhang <i>et al.</i> [15]	65 M	8.1	71.8	73.2	74.5	76.9	64.5	68.4	48.2	50.8	27.5	31.6	50.6	55.7	56.2	59.4
PGA-NET [16]	45 M	9.8	82.6	88.2	77.0	82.5	74.8	80.2	54.1	59.4	46.0	49.2	58.3	61.2	65.5	70.1
SCM-MRCNN	53 M	9.1	84.2	91.3	79.3	85.4	81.2	86.8	56.9	61.5	50.3	54.0	59.7	63.0	68.6	73.3

TABLE V: Quantitative comparison for the multi-class road defect detection and segmentation performance using RoadEYE dataset. The **bolded** numbers indicate the best performance.

we have compared our method with various SOTA instance segmentation methods [18], [19], [21], [57].

Table III compares defect segmentation performance using the CS and RoadEYE datasets. The SCM-MRCNN produces AID of 53.1, ODS of 64.5, and 69.0 OIS on the CS dataset. For the RoadEYE dataset, SCM-MRCNN produces AID of 22.6, ODS of 58.7, and 56.4 ODS on the CS dataset. These figures are the best performances in our experiments. Dual-Swin [18] produces the second-ranked performance. Interestingly, Dual-Swin also uses a self-attention module to learn a long-term dependency. Both Dual-Swin and SCM-MRCNN can learn features with spatially long-term dependencies through self-attention. These experimental results suggest that long-term dependencies help segment road defects.

Table IV compares multi-class defect detection performance using the RDD2020 and RoadEYE datasets. The SCM-MRCNN produces 63.5 precision, 60.9 recall, 61.5 F1-score, and 61.7 mAP on RDD2020 dataset. For the RoadEYE dataset, SCM-MRCNN produces 65.4 precision, 61.3 recall, 62.7 F1-score, and 63.1 mAP. These figures are the first-ranked performances in our experiments. Faster-RCNN [53] produces the second-ranked performance. Noticably, Region proposal-based methods [17], [53] including the proposed SCM-MRCNN show better performance than single-shot object detection-based methods [13], [55]. This suggests that the region-proposal modules can cover overall geometric information so that it helps identify various types of defects.

Performance comparisons with recent SOTA multi-class road deflection and segmentation and instant segmentation methods are presented in Table V. The SCM-MRCNN produces AP_M of 68.6, AP_B of 73.3. These figures are

the best performances in our experiments. However, for the Transverse crack class, the SCM-MRCNN produces second-ranked performances. Dual-Swin [18] produces better performance. The performance comparison results show that the SCM-MRCNN outperforms SOTA methods for road defect detection and instance segmentation.

For computational cost, the SCM-MRCNN has 53 million (M) parameters. This model size is relatively bigger than other MRCNN-based methods [17], [57] since the SCM-attention blocks have been embedded between each convolutional or deconvolutional layer, which make the network structure more complicated. However, it is smaller than YOLACT [21] and Centermask [19], which have over 100 M parameters. The method shows the fastest execution speed is YOLACT. The YOLACT shows 21.7 FPS. The SCM-MRCNN achieves 9.1 FPS, which is relatively slower than the YOLACT. However, the SCM-MRCNN obtains faster execution speed compared with Dual-Swin [18], and Centermask [57].

V. CONCLUSION

This paper presents an end-to-end framework for multi-class road defect detection and segmentation. To detect and segment multi-class road defects based on a single framework, it is essential to derive spatially and channel-wisely generalised representation. We design the spatial and channel-wise multi-head attention (SCM Attention) to learn better-generalised representation across all dimensions. The experimental results demonstrated the effectiveness of the SCM attention and the SCM-MRCNN for multi-class road defect detection and segmentation.

REFERENCES

- [1] Department of Transport (United Kingdom), "Road safety statistics," May 25, 2022. [Online]. Available: <https://www.gov.uk/government/statistical-data-sets/reported-road-accidents-vehicles-and-casualties-tables-for-great-britain>
- [2] H. Wang, I. Al-Saadi, P. Lu, and A. Jasim, "Quantifying greenhouse gas emission of asphalt pavement preservation at construction and use stages using life-cycle assessment," *International Journal of Sustainable Transportation*, vol. 14, no. 1, pp. 25–34, 2020.
- [3] I. Al-Saadi, H. Wang, X. Chen, P. Lu, and A. Jasim, "Multi-objective optimization of pavement preservation strategy considering agency cost and environmental impact," *International Journal of Sustainable Transportation*, vol. 15, no. 11, pp. 826–836, 2021.
- [4] I. Katsamenis, M. Bimpas, E. Protopapadakis, C. Zafeiropoulos, D. Kalogeras, A. Doulamis, N. Doulamis, C. Martín-Portugués Montoliu, Y. Handanos, F. Schmidt, *et al.*, "Robotic maintenance of road infrastructures: The heron project," in *Proceedings of the 15th International Conference on Pervasive Technologies Related to Assistive Environments*, 2022, pp. 628–635.
- [5] M. Eskandari Torbaghan, B. Kaddouh, M. Abdellatif, N. Metje, J. Liu, R. Jackson, C. Rogers, D. Chapman, R. Fuentes, M. Miodownik, *et al.*, "Application of robotic and autonomous systems for road defect detection and repair—a position paper on future road asset management."
- [6] S. Kornblith, M. Norouzi, H. Lee, and G. Hinton, "Similarity of neural network representations revisited," in *International conference on machine learning*. PMLR, 2019, pp. 3519–3529.
- [7] S. Li and X. Zhao, "Convolutional neural networks-based crack detection for real concrete surface," in *Sensors and Smart Structures Technologies for Civil, Mechanical, and Aerospace Systems 2018*, vol. 10598. SPIE, 2018, pp. 955–961.
- [8] J. Yu, K. C. Yow, and M. Jeon, "Joint representation learning of appearance and motion for abnormal event detection," *Machine Vision and Applications*, vol. 29, no. 7, pp. 1157–1170, 2018.
- [9] J. Yu, D. Y. Kim, Y. Lee, and M. Jeon, "Unsupervised pixel-level road defect detection via adversarial image-to-frequency transform," in *2020 IEEE Intelligent Vehicles Symposium (IV)*. IEEE, 2020, pp. 1708–1713.
- [10] R. Fan, M. J. Bocus, Y. Zhu, J. Jiao, L. Wang, F. Ma, S. Cheng, and M. Liu, "Road crack detection using deep convolutional neural network and adaptive thresholding," in *2019 IEEE Intelligent Vehicles Symposium (IV)*. IEEE, 2019, pp. 474–479.
- [11] D. Arya, H. Maeda, S. K. Ghosh, D. Toshniwal, and Y. Sekimoto, "Rdd2020: An annotated image dataset for automatic road damage detection using deep learning," *Data in brief*, vol. 36, p. 107133, 2021.
- [12] X. Zhang, X. Xia, N. Li, M. Lin, J. Song, and N. Ding, "Exploring the tricks for road damage detection with a one-stage detector," in *2020 IEEE International Conference on Big Data (Big Data)*. IEEE, 2020, pp. 5616–5621.
- [13] F. Wan, C. Sun, H. He, G. Lei, L. Xu, and T. Xiao, "Yolo-lrdd: A lightweight method for road damage detection based on improved yolov5s," *EURASIP Journal on Advances in Signal Processing*, vol. 2022, no. 1, p. 98, 2022.
- [14] Y. He, Z. Jin, J. Zhang, S. Teng, G. Chen, X. Sun, and F. Cui, "Pavement surface defect detection using mask region-based convolutional neural networks and transfer learning," *Applied Sciences*, vol. 12, no. 15, p. 7364, 2022.
- [15] K. Zhang, M. Zheng, Q. Yu, and Y. Liu, "Multi-class pavement disease recognition using object detection and segmentation," in *2022 12th International Conference on Information Science and Technology (ICIST)*. IEEE, 2022, pp. 211–216.
- [16] H. Dong, K. Song, Y. He, J. Xu, Y. Yan, and Q. Meng, "Pganet: Pyramid feature fusion and global context attention network for automated surface defect detection," *IEEE Transactions on Industrial Informatics*, vol. 16, no. 12, pp. 7448–7458, 2019.
- [17] K. He, G. Gkioxari, P. Dollár, and R. Girshick, "Mask r-cnn," in *Proceedings of the IEEE international conference on computer vision*, 2017, pp. 2961–2969.
- [18] T. Liang, X. Chu, Y. Liu, Y. Wang, Z. Tang, W. Chu, J. Chen, and H. Ling, "Cbnet: A composite backbone network architecture for object detection," *IEEE Transactions on Image Processing*, vol. 31, pp. 6893–6906, 2022.
- [19] Y. Lee and J. Park, "Centermask: Real-time anchor-free instance segmentation," in *Proceedings of the IEEE/CVF conference on computer vision and pattern recognition*, 2020, pp. 13 906–13 915.
- [20] Q. Zou, Y. Cao, Q. Li, Q. Mao, and S. Wang, "Cracktree: Automatic crack detection from pavement images," *Pattern Recognition Letters*, vol. 33, no. 3, pp. 227–238, 2012.
- [21] D. Bolya, C. Zhou, F. Xiao, and Y. J. Lee, "Yolact: Real-time instance segmentation," in *Proceedings of the IEEE/CVF international conference on computer vision*, 2019, pp. 9157–9166.
- [22] Q. Li and X. Liu, "Novel approach to pavement image segmentation based on neighboring difference histogram method," in *2008 Congress on Image and Signal Processing*. IEEE, pp. 792–796. [Online]. Available: <http://ieeexplore.ieee.org/document/4566413/>
- [23] N. Tanaka and K. Uematsu, "A crack detection method in road surface images using morphology," pp. 154–157.
- [24] Y. Maode, B. Shaobo, X. Kun, and H. Yuyao, "Pavement crack detection and analysis for high-grade highway," in *2007 8th International Conference on Electronic Measurement and Instruments*. IEEE, pp. 4–548–4–552. [Online]. Available: <http://ieeexplore.ieee.org/document/4351202/>
- [25] N. T. Sy, M. Avila, S. Begot, and J. C. Bardet, "Detection of defects in road surface by a vision system," in *MELECON 2008 - The 14th IEEE Mediterranean Electrotechnical Conference*. IEEE, pp. 847–851. [Online]. Available: <http://ieeexplore.ieee.org/document/4618541/>
- [26] N. T. Nguyen, M. Avila, and S. Begot, "Automatic detection and classification of defect on road pavement using anisotropy measure," in *2009 17th European Signal Processing Conference*, pp. 617–621. [Online]. Available: <https://ieeexplore.ieee.org/abstract/document/7077799>
- [27] H. Oliveira and P. Lobato, "Supervised crack detection and classification in images of road pavement flexible surfaces," in *Recent Advances in Signal Processing*, A. A, Ed. InTech. [Online]. Available: <http://www.intechopen.com/books/recent-advances-in-signal-processing/supervised-crack-detection-and-classification-in-images-of-road-pavement-flexible-surfaces>
- [28] A. Cord and S. Chambon, "Automatic road defect detection by textural pattern recognition based on AdaBoost: Automatic road defect detection," vol. 27, no. 4, pp. 244–259. [Online]. Available: <https://onlinelibrary.wiley.com/doi/10.1111/j.1467-8667.2011.00736.x>
- [29] L. Breiman, "Random forests," vol. 45, no. 1, pp. 5–32. [Online]. Available: <https://doi.org/10.1023/A:1010933404324>
- [30] P. Prasanna, K. J. Dana, N. Gucunski, B. B. Basily, H. M. La, R. S. Lim, and H. Parvardeh, "Automated crack detection on concrete bridges," vol. 13, no. 2, pp. 591–599. [Online]. Available: <http://ieeexplore.ieee.org/document/6917066/>
- [31] M. S. Kaseko and S. G. Ritchie, "A neural network-based methodology for pavement crack detection and classification," vol. 1, no. 4, pp. 275–291. [Online]. Available: <https://www.sciencedirect.com/science/article/pii/S0968090X9390002W>
- [32] S. Liu, J. Huang, J. Sung, and C. Lee, "Detection of cracks using neural networks and computational mechanics," vol. 191, pp. 2831–2845.
- [33] J. Zhong, Z. Liu, Z. Han, Y. Han, and W. Zhang, "A CNN-based defect inspection method for catenary split pins in high-speed railway," vol. 68, no. 8, pp. 2849–2860. [Online]. Available: <https://ieeexplore.ieee.org/document/8482333/>
- [34] J. Yu, H. Oh, S. Fichera, P. Paoletti, and S. Luo, "Multi-source domain adaptation for unsupervised road defect segmentation," in *2023 IEEE International Conference on Robotics and Automation (ICRA)*. IEEE, 2023, pp. 5638–5644.
- [35] W. Qiao, Q. Liu, X. Wu, B. Ma, and G. Li, "Automatic pixel-level pavement crack recognition using a deep feature aggregation segmentation network with a scSE attention mechanism module," vol. 21, no. 9, p. 2902, number: 9 Publisher: Multidisciplinary Digital Publishing Institute. [Online]. Available: <https://www.mdpi.com/1424-8220/21/9/2902>
- [36] J. C. Ong, S. L. Lau, M.-Z. Ismadi, and X. Wang, "Feature pyramid network with self-guided attention refinement module for crack segmentation," vol. 22, no. 1, pp. 672–688, publisher: SAGE Publications. [Online]. Available: <https://doi.org/10.1177/14759217221089571>
- [37] J. König, M. David Jenkins, P. Barrie, M. Mannion, and G. Morison, "A convolutional neural network for pavement surface crack segmentation using residual connections and attention gating," in *2019 IEEE International Conference on Image Processing (ICIP)*, pp. 1460–1464, ISSN: 2381-8549.
- [38] A. Vaswani, N. Shazeer, N. Parmar, J. Uszkoreit, L. Jones, A. N. Gomez, L. Kaiser, and I. Polosukhin, "Attention is all you need." [Online]. Available: <http://arxiv.org/abs/1706.03762>

- [39] H. Liu, X. Miao, C. Mertz, C. Xu, and H. Kong, "CrackFormer: Transformer network for fine-grained crack detection," in *2021 IEEE/CVF International Conference on Computer Vision (ICCV)*. IEEE, pp. 3763–3772. [Online]. Available: <https://ieeexplore.ieee.org/document/9711107/>
- [40] F. Guo, Y. Qian, J. Liu, and H. Yu, "Pavement crack detection based on transformer network," vol. 145, p. 104646. [Online]. Available: <https://linkinghub.elsevier.com/retrieve/pii/S0926580522005167>
- [41] E. Asadi Shamsabadi, C. Xu, A. S. Rao, T. Nguyen, T. Ngo, and D. Dias-da Costa, "Vision transformer-based autonomous crack detection on asphalt and concrete surfaces," vol. 140, p. 104316. [Online]. Available: <https://linkinghub.elsevier.com/retrieve/pii/S0926580522001893>
- [42] W. Wang and C. Su, "Automatic concrete crack segmentation model based on transformer," vol. 139, p. 104275. [Online]. Available: <https://www.sciencedirect.com/science/article/pii/S0926580522001480>
- [43] R. Girshick, J. Donahue, T. Darrell, and J. Malik, "Rich feature hierarchies for accurate object detection and semantic segmentation," in *2014 IEEE Conference on Computer Vision and Pattern Recognition*, 2014, pp. 580–587.
- [44] R. Girshick, "Fast r-CNN." [Online]. Available: <http://arxiv.org/abs/1504.08083>
- [45] S. Ren, K. He, R. Girshick, and J. Sun, "Faster r-CNN: Towards real-time object detection with region proposal networks," vol. 39, no. 6, pp. 1137–1149.
- [46] X. Xu, M. Zhao, P. Shi, R. Ren, X. He, X. Wei, and H. Yang, "Crack detection and comparison study based on faster r-CNN and mask r-CNN," vol. 22, no. 3, p. 1215. [Online]. Available: <https://www.mdpi.com/1424-8220/22/3/1215>
- [47] W. Wang, B. Wu, S. Yang, and Z. Wang, "Road damage detection and classification with faster r-CNN," in *2018 IEEE International Conference on Big Data (Big Data)*. IEEE, pp. 5220–5223. [Online]. Available: <https://ieeexplore.ieee.org/document/8622354/>
- [48] D. Li, Q. Xie, X. Gong, Z. Yu, J. Xu, Y. Sun, and J. Wang, "Automatic defect detection of metro tunnel surfaces using a vision-based inspection system," vol. 47, p. 101206. [Online]. Available: <https://linkinghub.elsevier.com/retrieve/pii/S1474034620301750>
- [49] H. Nam and H.-E. Kim, "Batch-instance normalization for adaptively style-invariant neural networks," *Advances in Neural Information Processing Systems*, vol. 31, 2018.
- [50] Ç. F. Özgenel and A. G. Söğüt, "Performance comparison of pretrained convolutional neural networks on crack detection in buildings," in *Isarc. proceedings of the international symposium on automation and robotics in construction*, vol. 35. IAARC Publications, 2018, pp. 1–8.
- [51] K. Liu, G. Yang, J. Zhang, Z. Zhao, X. Chen, and B. M. Chen, "Datasets and methods for boosting infrastructure inspection: A survey on defect segmentation and detection," in *2022 IEEE 17th international conference on control & automation (ICCA)*. IEEE, 2022, pp. 23–30.
- [52] Y. Liu, M.-M. Cheng, X. Hu, K. Wang, and X. Bai, "Richer convolutional features for edge detection," in *Proceedings of the IEEE conference on computer vision and pattern recognition*, 2017, pp. 3000–3009.
- [53] J. Long, E. Shelhamer, and T. Darrell, "Fully convolutional networks for semantic segmentation," in *Proceedings of the IEEE conference on computer vision and pattern recognition*, 2015, pp. 3431–3440.
- [54] F. Yang, L. Zhang, S. Yu, D. Prokhorov, X. Mei, and H. Ling, "Feature pyramid and hierarchical boosting network for pavement crack detection," *IEEE Transactions on Intelligent Transportation Systems*, 2019.
- [55] O. Ronneberger, P. Fischer, and T. Brox, "U-net: Convolutional networks for biomedical image segmentation," in *International Conference on Medical image computing and computer-assisted intervention*. Springer, 2015, pp. 234–241.
- [56] D. Arya, H. Maeda, S. K. Ghosh, D. Toshniwal, H. Omata, T. Kashiya, and Y. Sekimoto, "Global road damage detection: State-of-the-art solutions," in *2020 IEEE International Conference on Big Data (Big Data)*. IEEE, 2020, pp. 5533–5539.
- [57] L. Ke, M. Danelljan, X. Li, Y.-W. Tai, C.-K. Tang, and F. Yu, "Mask transfiner for high-quality instance segmentation," in *Proceedings of the IEEE/CVF Conference on Computer Vision and Pattern Recognition*, 2022, pp. 4412–4421.